Cell Calcium 77 (2019) 1–7

Contents lists available at ScienceDirect

Cell Calcium

journal homepage: www.elsevier.com/locate/ceca

Effects of his-tags on physical properties of parvalbumins

Alisa A. Vologzhannikova[a], Polina A. Khorn[a], Alexei S. Kazakov[a], Eugene A. Permyakov[a,**], Vladimir N. Uversky[a,b,*], Sergei E. Permyakov[a,**]

[a] Institute for Biological Instrumentation of the Russian Academy of Sciences, Pushchino, Moscow region, 142290, Russia
[b] Department of Molecular Medicine and USF Health Byrd Alzheimer's Research Institute, Morsani College of Medicine, University of South Florida, Tampa, Florida 33612, USA

ARTICLE INFO

Keyword:
Protein

ABSTRACT

A comparative study of His-tagged and non-tagged rat β-parvalbumin (rWT β-PA), calcium binding protein with the EF-hand calcium binding domains, has been carried out. The attachment of His-tag increases α-helical content and decreases β-sheets and β-turns content of the metal free form (apo-state) of β-PA. In contrast to this, the attachment of His-tag decreases α-helical content by more than 10% and increases contents of β-sheets and β-turns of the Ca^{2+}-loaded state. According to the dynamic light scattering analysis, apo-state of His-tagged rat β-PA seems to be less compact compared with the apo-state of non-tagged rat β-PA. Surprisingly, the attachment of His-tag practically does not change mean hydrodynamic radius of Ca^{2+}-loaded rat β-PA. The attachment of His-tag shifts thermal denaturation peaks of both apo- and Ca^{2+}-loaded states of rat β-PA towards higher temperatures by 3–4 °C and slightly decreases its Ca^{2+} affinity. These results should be taken into consideration in the use of His-tagged parvalbumins.

1. Introduction

Poly-histidine-tag at the N- or C-terminus of a protein is an artificial amino acid motif, which consists of at least six histidine residues [1]. Poly-histidine tags are most often used for affinity purification of recombinant proteins expressed in prokaryotic expression systems [2–4]. Ni-affinity chromatography uses the ability of His to bind nickel, which is bound to an agarose bead by chelation using nitroloacetic acid (NTA) beads. The general method is to apply the poly-histidine-tagged protein onto the column, by mixing the beads with the sample, then pouring the slurry of NTA beads and protein into a column. Low concentrations of phosphate and imidazole buffers are used to remove low affinity bound proteins. Finally, higher concentrations of imidazole are used to elute the target protein from the NTA-beads. The use of His-tags essentially simplifies the process of protein purification. At the same time, physical properties of His-tagged proteins can be different from those of the non-tagged proteins. In the present work we carried out a comparative study of His-tagged and non-tagged parvalbumins, calcium binding proteins with the EF-hand calcium binding domains.

Parvalbumins are small (molecular mass about 12 kDa), acidic (pI 3.5–5.0) cytosolic proteins contained in large concentrations in fast skeletal and sometimes in cardiac muscles, some types of neurons and cells of several endocrine glands (for review see, for example, [5–7]). Parvalbumin possesses two active EF-hand Ca^{2+} binding sites formed by the CD and EE loops with flanking α-helices (CD and EF domains, respectively) (reviewed in [5]). The AB domain of PA cannot bind Ca^{2+} due to the shortened AB-loop and disturbed Ca^{2+} binding DxDxDG motif. Sometimes His-tags are used for fast and effective extraction and purification of PAs. In this study, we have compared structural, conformational and functional properties of His-tagged and non-tagged PAs and found that some essential physical properties of these PA forms are different, and this fact should be taken into consideration in the use of His-tagged proteins.

2. Materials and methods

2.1. Materials

Molecular biology grade HEPES, ultra-grade H_3BO_3/glycine/Tris were from Calbiochem, Fluka, Sigma-Aldrich Co., and Amresco, respectively. Pharma grade KCl and ultra-grade TCA were purchased from Panreac AppliChem. Biotechnology grade DTT was purchased from

* Corresponding author at: Department of Molecular Medicine, Morsani College of Medicine, University of South Florida, Tampa, FL 33612, USA.
** Corresponding authors at: Institute for Biological Instrumentation of the Russian Academy of Sciences, Institutskaya str., 7, Pushchino, Moscow region 142290, Russia.
E-mail addresses: permyakov.s@gmail.com (E.A. Permyakov), vuversky@health.usf.edu (V.N. Uversky), epermyak@yandex.ru (S.E. Permyakov).

https://doi.org/10.1016/j.ceca.2018.11.006
Received 18 October 2018; Received in revised form 14 November 2018; Accepted 14 November 2018
Available online 16 November 2018
0143-4160/

DiaM (Moscow, Russia). Biotechnology grade 2-ME and molecular mass markers for SDS-PAGE were from Helicon (Moscow, Russia). Ultra-grade KOH, EDTA and standard solutions of $CaCl_2$ were purchased from Sigma-Aldrich Co. Standard solutions of EDTA potassium salt was prepared as described in [8]. Molecular biology grade glutaric aldehyde was from Amersham Biosciences. Biochemistry grade Coomassie Brilliant Blue R-250 was products of Merck. Toyopearl SuperQ-650 M was purchased from Tosoh Bioscience. Sephadex G-25 and PD MidiTrap™ G-25 were products of Pharmacia LKB and GE Healthcare, respectively. D-10-camphorsulfonic acid was from JASCO, Inc. Other chemicals were reagent grade or higher.

All buffers and other solutions were prepared using ultrapure water (Millipore Simplicity 185 system). Plastics or quartz ware were used instead of glassware, to avoid contamination of protein samples with Ca^{2+}. DTT solutions were prepared using degassed buffers immediately prior to the usage to avoid DTT oxidation. Thermo SnakeSkin dialysis tubing (3.5 kDa MWCO) and Millipore Amicon Ultra centrifugal filters (3.0 kDa MWCO) were used for dialysis and concentration of protein solutions, respectively.

2.2. Expression and purification of rWT β-PA and rWT His-tag β-PA

Recombinant wild-type rat (*Rattus norvegicus*) β-parvalbumin (rWT β-PA) was isolated and purified as described earlier [9]. The rat rWT β-PA gene was cloned into pET28a vector between the *XhoI* and *XbaI* restriction sites. The resulting gene contained 6xHis-tag at the C-terminal end (rWT His-tag β-PA). The tagged rWT His-tag β-PA was expressed and purified similarly to rWT β-PA since the classical method of affinity purification of poly-histidine-tagged proteins provides low yield of the protein. In our work, the yield was 40–60 mg of protein per liter of cell culture for both β-PA samples. Purity of the protein samples was confirmed by native and SDS-PAGE and characteristic UV absorption and fluorescence spectra (rat β-PA contains Tyr and Phe residues, but lacks Trp). Both purified β-PA samples were exhaustively dialyzed against distilled water with 1 mM 2-ME at 4 °C, freeze-dried and stored at −20 °C. Before experiments, the dried β-PAs (rWT β-PA and rWT His-tag β-PA) were dissolved in distilled water, reduced by addition of freshly prepared 5 mM DTT and purified from 2-ME and DTT by passage through PD MidiTrap G-25 column equilibrated with a buffer of choice. The reduced protein was used for experiments as soon as possible. Molecular masses of the reduced β-PA samples were checked by electrospray ionization mass spectrometry (ESI-MS) coupled with reverse-phase high performance liquid chromatography as described in [10]. The sample of 0.5 μM β-PA in 15:75 (v/v) mixture of deionized water and acetonitrile (10 mM formic acid) was purified using HPLC in an Easy-nLC 1000 (Thermo Scientific, United States) nanoflow liquid chromatograph in a column filled with C18 sorbent (granule diameter was 2.7 μm and pore size was 300 Å) in 15–100% acetonitrile gradient for 220 min at flow rate 0.25 μL/min. Mass spectra were measured by Orbitrap Elite mass spectrometer. Acquisition was carried out in a positive ion mode from 600 to 2000 *m/z* at detector voltage 1.8 kV, capillary temperature 240 °C and nebulizing nitrogen flow 1.0 l/min. β-PA concentrations were calculated spectrophotometrically using the molar extinction coefficient at 280 nm, ε_{280nm}, derived from the molar extinction coefficients at 205 nm estimated according to [11]: 2409 $M^{-1}\,cm^{-1}$ and 2721 $M^{-1}\,cm^{-1}$ for apo- and metal-loaded rWT β-PA, respectively; 2423 $M^{-1}\,cm^{-1}$ and 2486 $M^{-1}\,cm^{-1}$ for apo- and metal-loaded rWT His-tag β-PA, respectively.

2.3. Removal of metal ions from β-PAs

The contaminating Ca^{2+}/Mg^{2+} ions were removed from β-PAs via precipitation by TCA [12] of the preliminary reduced protein (see above) (10 mM HEPES-KOH, pH 8.2 or 20 mM H_3BO_3-KOH, pH 8.4 buffer), followed by purification from Ca^{2+}/Mg^{2+} and TCA by gel-filtration method [13] using Sephadex G-25 column equilibrated with a respective buffer. To protect the reduced proteins from oxidation, 5 mM freshly prepared DTT solution was added prior to the precipitation by TCA and before the gel-filtration. This procedure was used for metal removal from rWT β-PA and rWT His-tag β-PA for CD measurements of apo-form β-PAs, chemical cross-linking and DLS measurements and metal affinity studies. Only the gel-filtration method [13] was used for CD measurements of Ca^{2+}-loaded β-PAs, DSC measurements of apo- and Ca^{2+}-loaded β-PAs.

2.4. Circular dichroism measurements

Circular dichroism (CD) studies were carried out with a *J*-810 spectropolarimeter (JASCO, Inc.), equipped with a Peltier-controlled cell holder. The instrument was calibrated with an aqueous solution of D-10-camphorsulfonic acid according to the manufacturer's instruction. The cell compartment was purged with nitrogen (dew-point of –40 °C). The quartz cell with path length of 1.00 mm was used for far-UV measurements. Protein concentration was 5–11 μM. Buffer conditions: 10 mM H_3BO_3-KOH, pH 8.8, 1.5 mM EDTA or 1 mM $CaCl_2$ (for apo- and Ca^{2+}-loaded proteins, respectively); 20 °C A small contribution of buffer was subtracted from experimental spectra. Band width was 2 nm, averaging time 2 s, and accumulation 3. Quantitative estimates of the secondary structure contents were carried out using the CDPro software package [14] (http://lamar.colostate.edu/~sreeram/CDPro/main.html). SELCON3, CDSSTR and CONTIN algorithms were used for evaluation of secondary structure fractions. SDP48 and SMP56 reference protein sets were used for these evaluations. The final secondary structure fractions represent averaged values.

2.5. Scanning calorimetry measurements

Differential scanning calorimetry (DSC) studies were carried out on a Nano DSC microcalorimeter (TA Instruments) at a 1 K/min heating rate and excess pressure of 4 bar. β-PA concentrations were 1.0–2.1 mg/ml. Buffer conditions: 10 mM H_3BO_3-KOH, 1 mM $CaCl_2$, pH 9.0 for Ca^{2+}-bound β-PA and 20 mM glycine-KOH, pH 9.2, 1 mM EDTA for apo-β-PA. The DSC measurements and calculations of protein specific heat capacity (C_p) were performed as described in [10]. The partial molar volume of β-PA and specific heat capacity of the fully unfolded protein were estimated according to [15] and [16], respectively. The temperature dependence of C_p was analyzed according to the *co-operative two-state* model:

$$n{\cdot}N \leftrightarrow n{\cdot}D \quad (I)$$

where N and D denote native and denatured protein states, respectively; *n* is a number of molecules involved in the transition. The experimental data were fitted by the equations derived earlier [17] using Microcal OriginPro 8.0 (Origin Lab Corporation, Northampton, MA, USA) software. The heat capacity change accompanying the thermal transition (ΔC_p) was supposed to be independent of temperature. ΔC_p, mid-transition temperature (T_m), enthalpy of protein denaturation at temperature T_m (ΔH_0), and n were used as fitting parameters (in some cases n was set to 1).

2.6. Dynamic light scattering studies

Dynamic light scattering (DLS) measurements were carried out at 20 °C using a Zetasizer Nano ZS system (Malvern Instruments Ltd.). The backscattered light of a 4 mW He-Ne laser (632.8 nm) was collected at an angle of 173°. Concentration of β-PA in these experiments was 1.5 mg/ml. Before the measurements the protein samples were passed through 0.02 μm Whatman Anotop 10 syringe filters. The following buffer conditions were used: 20 mM H_3BO_3-KOH, pH 8.4, 1.5 mM EDTA (for apo-proteins) or 1 mM $CaCl_2$ (for Ca^{2+}-loaded proteins). Acquisition time for a single autocorrelation function was 100 s. The

resulting autocorrelation functions were averaged values from ten measurements. The intensity-weighted size distributions were calculated using preset parameters for distilled water at 20 °C (refractive index of 1.33 and a viscosity value of 1.0031 cP). The estimates of mean hydrodynamic radii of PAs were derived from these distributions. Apparent molecular weights of parvalbumins were calculated using Mark-Houwink equation, as implemented for proteins in the Zetasizer Nano ZS software.

2.7. Chemical crosslinking of β-PAs

Protein (1.5 mg/ml) crosslinking with 0.02% glutaric aldehyde was performed in 20 mM H_3BO_3-KOH, pH 8.4; 1.5 mM EDTA (for apo-proteins) or 1 mM $CaCl_2$ (for Ca^{2+}-loaded proteins). The reaction proceeded for 16 h at 15 °C and was stopped by addition of 4-fold volume of the buffer used in SDS PAAG electrophoresis. The samples were subjected to SDS-PAGE (5% concentrating and 15% resolving gels; 5 μg of β-PA per lane) and stained with Coomassie Brilliant Blue R-250. The gels were scanned using Molecular Imager PharosFX Plus System (Bio-Rad Laboratories, Inc.) and analyzed by Quantity One software.

2.8. Intrinsic fluorescence measurements

Fluorescence studies were performed with a Cary Eclipse spectrofluorimeter (Varian, Inc.), equipped with a Peltier-controlled cell holder. Quartz cells with path length of 10 mm were used. Protein concentrations were 10–16 μM. Buffer conditions: 10 mM HEPES-KOH, pH 8.2. Fluorescence of Tyr residues of PAs was excited at 275 nm. In titration experiments, all spectra were corrected for dilution according to the equation:

$$F_\lambda \times (1 - 10^{-D}0) / (1 - 10^{-D}0^{/k}) \quad (1)$$

where F_λ denotes protein fluorescence intensity at a wavelength λ, D_0 is absorption of β-PAs at the excitation wavelength, k is dilution coefficient.

2.9. Calcium binding measurements

The binding of Ca^{2+} ions to rat β-PA can be described by a sequential Ca^{2+}-binding scheme [18]:

$$P + M \overset{K_a1}{\leftrightarrow} P{\cdot}M, \qquad P{\cdot}M + M \overset{K_a2}{\leftrightarrow} P{\cdot}M_2, \quad (II)$$

where K_1 and K_2 are equilibrium Ca^{2+}-binding constants for the two active EF-hands of parvalbumin. The calcium affinity of β-PA was estimated from a spectrofluorimetric titration of the Ca^{2+}-free protein with a $CaCl_2$ standard followed by a spectrofluorimetric titration of the Ca^{2+}-loaded protein with EDTA potassium salt at a fixed pH. Calculations of the Ca^{2+} association constants from the experimental data were performed using a competition between the protein and the chelator for Ca^{2+} ions, which is described by the scheme (II) with the addition of equilibrium (III):

$$EDTA + M \overset{K_{EDTA}}{\leftrightarrow} EDTA{\cdot}M \quad (III)$$

The Ca^{2+} association constant for EDTA, K_{EDTA}, was calculated according to [19]. The experimental data were globally fitted using FluoTitr v.1.2 software [20]. The fit was achieved by variation of the binding constants K_1 and K_2. The quality of the fit was judged by the randomness of residuals distribution. The resulting accuracy of the Ca^{2+}-binding constants was about ± 1/4 orders of their magnitudes.

2.10. Evaluation of intrinsic disorder predisposition of rat β-parvalbumin and its C-terminally His-tagged form

Intrinsic disorder predisposition of rat β-parvalbumin (UniProt ID: P02631) and its C-terminally His-tagged form were evaluated using several commonly utilized disorder predictors, such as PONDR® VLXT [21], PONDR® VSL2 [22], PONDR® VL3 [22,23], PONDR® FIT [24], IUPred_short, and IUPred_long [25,26]. Justification for the selection of these tools is provided in our previous publications (e.g. [27,28],). We also generated a mean per-residue intrinsic disorder profile for a given protein by averaging the outputs of these six per-residue disorder predictors, and this mean disorder profile was also added to the corresponding plot. Use of consensus for evaluation of intrinsic disorder is motivated by empirical observations that this approach usually increases the predictive performance compared to the use of a single predictor [29–31]. The outputs of the evaluation of the per-residue disorder propensity by these tools are represented as the real numbers between 1 (ideal prediction of disorder) and 0 (ideal prediction of order). A threshold of ≥0.5 was used to identify disordered residues and regions in query proteins, whereas residues/regions characterized by the disorder scores ranging from 0.2 to 0.5 are classified as flexible.

2.11. Search for intrinsic disorder-based binding sites in rat β-parvalbumin and its C-terminally His-tagged form

Many intrinsically disordered proteins or proteins containing intrinsically disordered regions possess disorder-based binding sites, known as molecular recognition features (MoRFs) [32–35], which are located within longer IDPRs, are mostly disordered in their unbound states, but can undergo disorder-to-order transitions at interaction with specific binding partners [36–38]. Such potential disorder-based protein binding sites in rat β-parvalbumin and its C-terminally His-tagged form were identified by the ANCHOR algorithm [39,40]. This algorithm utilizes the pair-wise energy estimation approach originally used by IUPred [25,26], This approach acts on the hypothesis that long regions of disorder include localized potential binding sites which are not capable of folding on their own due to not being able to form enough favorable intrachain interactions, but can obtain the energy to stabilize via interaction with a globular protein partner [39,40].

3. Results and discussion

We produced recombinant non-tagged and His-tagged rat β-parvalbumin (rWT β-PA and rWT His-tag β-PA, respectively) and studied physical properties of their metal-free (apo-) and Ca^{2+}-loaded states. Electrospray ionization mass spectrometry (ESI-MS) measurements revealed the two major fractions of rWT β-PA samples. One of them (*ca* 45%) had a mass of 12,057 Da, which is consistent with the mass of the reduced form of a protein (UniProt entry P02631) without Met1 residue and N-terminal acetyl group. The other rWT β-PA fraction (*ca* 46%) was 131 Da heavier, in line with the presence of Met1 residue. The minor fractions (*ca* 9%) of this protein corresponded to Ca^{2+}-bound and oxidized states of the aforementioned forms. Similar data were obtained for rWT His-tag β-PA samples (with and without Met1 residue) but the contribution of the Ca^{2+}-bound and oxidized states was about 50%. Experiments on chemical crosslinking of the protein samples with 0.02% glutaric aldehyde (15 °C) showed that apo- and Ca^{2+}-loaded states of both non-tagged and His-tagged rat β-PA were monomeric.

Secondary structure of the non-tagged and His-tagged rat β-PA in various states was evaluated by circular dichroism method. Far-UV circular dichroism spectra for apo (1.5 mM EDTA), Mg^{2+}- (1 mM EGTA, 1 mM $MgCl_2$) and Ca^{2+}-loaded (1 mM $CaCl_2$) forms of rWT β-PA and its His-tagged mutant, rWT His-tag β-PA, at 20 °C are shown on Fig. 1. These spectra were used to evaluate the secondary structure composition of different forms of this protein (see Table 1). It is clearly seen that the His-tag grafting changes the secondary structure of rat β-PA,

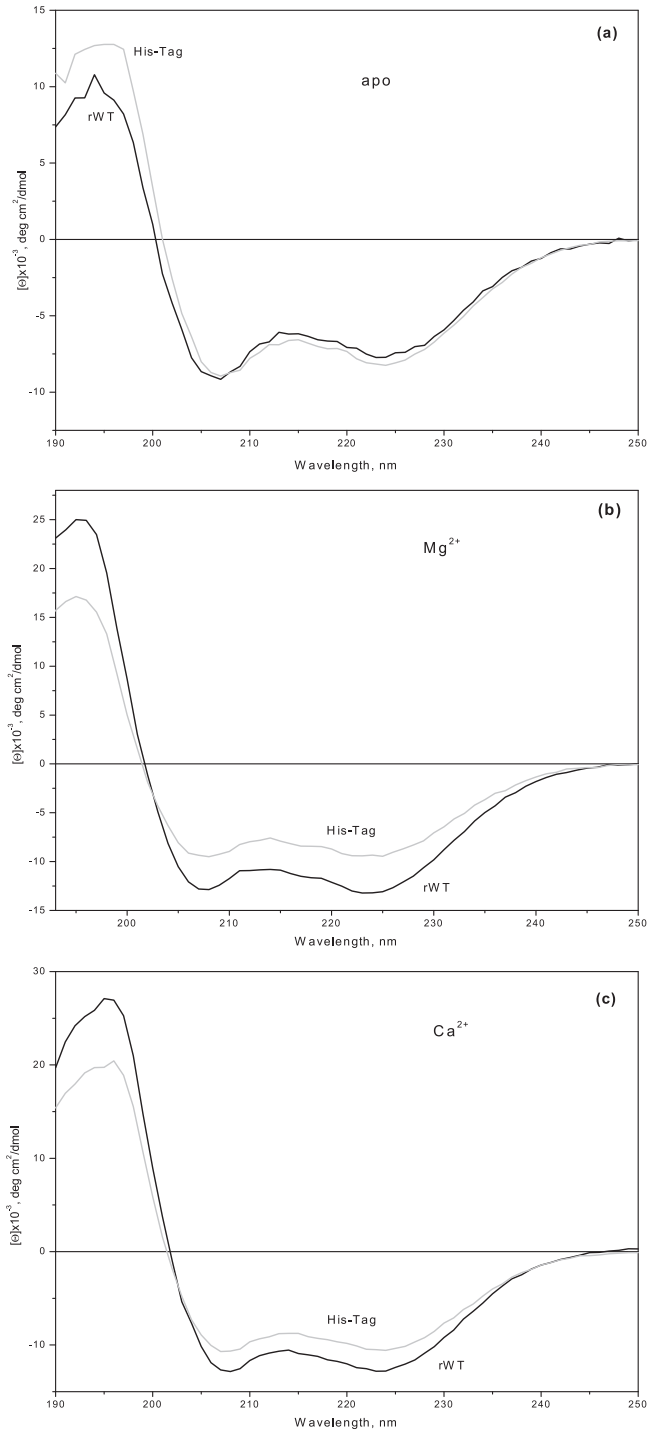

Fig. 1. Far-UV circular dichroism (CD) data for apo (1.5 mM EDTA), Mg^{2+}-(1 mM EGTA, 1 mM $MgCl_2$) and Ca^{2+}-loaded (1 mM $CaCl_2$) forms of rWT β-PA of rat and its His-tagged mutant rWT His-tag β-PA at 20 °C. Buffer conditions: 10 mM H_3BO_3, pH 8.8.

causing increase in the α-helical content and decrease in the β-sheet and β-turn contents of the apo-state (Table 1). At the same time, according to the dynamic light scattering (DLS) data (Table 2), mean hydrodynamic radius of the apo-state of rWT His-tag β-PA is 0.05 nm larger than that of the apo-state of the non-tagged rat β-PA, which means that it is slightly less compact. It is of interest to compare the measured R_S values of the WT and His-tagged rat β-PA with those calculated for the various conformations of globular protein of comparable molecular masses. According to a set of equations correlating

Table 1
Contributions of the secondary structure elements to the far UV CD spectra of apo (1.5 mM EDTA), and Ca^{2+}-loaded (1 mM $CaCl_2$) states of rat rWT β-PA and its His-tagged mutant rWT His-tag β-PA at 20 °C. Protein concentration was 5–11 μM. Buffer conditions: 10 mM H_3BO_3-KOH, pH 8.8. Decomposition of the CD spectra was carried out by CDRpro software (http://lamar.colostate.edu/~sreeram/CDPro/main.html. Standard deviations for mean estimation of secondary structure contributions are shown.

Protein	Protein state	α-helices	β-sheets	β-turns	random coil
rWT β-PA	apo-state	32.4 ± 4.3	17.1 ± 3.0	17.4 ± 0.8	30.2 ± 0.9
rWT His-tag β-PA		37.2 ± 3.5	15.7 ± 4.7	14.4 ± 3.9	31.4 ± 3.1
rWT β-PA	Ca^{2+}-loaded	54.8 ± 4.3	8.0 ± 3.04	12.1 ± 0.8	24.7 ± 0.9
rWT His-tag β-PA		43.7 ± 5.8	10.7 ± 2.0	17.8 ± 1.7	27.3 ± 4.4

Table 2
Mean hydrodynamic radius (R_S) of apo (1.5 mM EDTA) and Ca^{2+}-loaded (1 mM $CaCl_2$) states of rat rWT β-PA and its His-tagged mutant rWT His-tag β-PA at 15 °C measured by DLS (20.0 °C). Rat β-PAs concentration was 1.5 mg/ml. Buffer conditions: 20 mM H_3BO_3-KOH pH 8.4.

PA	Protein state	DLS data	
		R_S, nm	MW/MW_m
rWT β-PA	apo	2.18 ± 0.05	1.69 ± 0.12
rWT His-tag β-PA		2.23 ± 0.04	1.65 ± 0.11
rWT β-PA	Ca^{2+}-loaded	1.76 ± 0.03	0.98 ± 0.15
rWT His-tag β-PA		1.76 ± 0.02	0.97 ± 0.04

the R_S values with molecular masses of globular proteins in various conformations, the native states of proteins with molecular masses of the WT and His-tagged rat β-PA (12,057.12 and 13,122.24 Da, respectively) are expected to have the R_S values of 17.9 Å and 18.5 Å, the molten globular forms of such proteins should have the R_S values of 20.4 Å and 21.0 Å, their pre-molten globular word are expected to be characterized by the R_S values of 24.5 Å and 25.4 Å, whereas the GdmCl-unfolded forms should have the R_S values of 31.1 Å and 32.6 Å. This places the measured R_S values (21.8 ± 0.5 and 22.3 ± 0.4 Å) between the R_S values evaluated for the molten globular and pre-molten globular states of proteins with molecular masses of the WT and His-tagged rat β-PA.

In contrast to the aforementioned effects of the His-tag grafting on structural properties of apo-form of rat β-PA, attachment of His-tag decreases α-helical content (more than 10% change) and increases content of β-sheets and β-turns of the Ca^{2+}-loaded state of the rWT His-tag β-PA (Table 1). This means that His-tag perturbs structure of the Ca^{2+}-loaded states of rat β-PA. Surprisingly, the attachment of His-tag does not change mean hydrodynamic radius of Ca^{2+}-loaded rat β-PA (Table 2), and the measured R_S value (17.6 Å) corresponded well to the R_S value estimated for a native state of a protein with corresponding molecular mass.

Fig. 2 shows temperature dependencies of specific heat capacities of apo- and Ca^{2+}-bound states for rat rWT β-PA and its His-tagged mutant rWT His-tag β-PA derived from the differential scanning calorimetry (DSC) data. Thermodynamic parameters of thermal denaturation of various forms of rat β-PA estimated from these DSC data are collected in Table 3. The grafting of His-tag makes the protein more resistant to thermal denaturation, shifting the thermal transition peaks of both apo- and Ca^{2+}-loaded states towards higher temperatures by 3 to 4 °C. The shape of the heat sorption peak for Ca^{2+}-loaded rWT His-tag β-PA suggests that its thermal denaturation is accompanied by protein aggregation, and this process decreases the magnitude of the high temperature shift of the heat sorption peak.

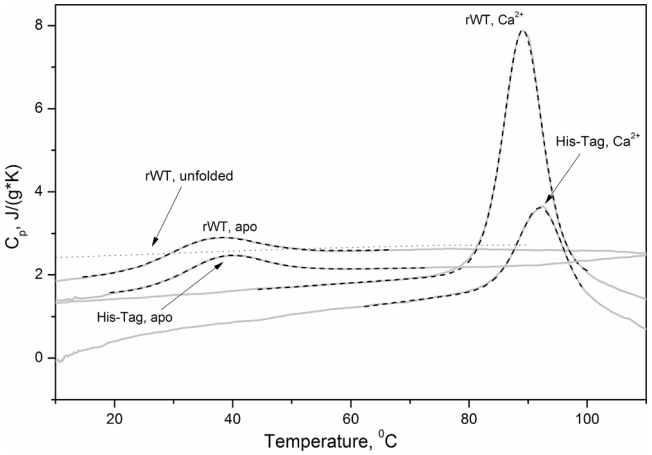

Fig. 2. Temperature dependencies of specific heat capacities of apo- and Ca^{2+}-bound states for rWT β-PA of rat and its His-tagged mutant rWT His-tag β-PA derived from DSC data. Protein concentration was 1.0–2.1 mg/ml. Buffer conditions: 10 mM H_3BO_3-KOH, 1 mM $CaCl_2$, pH 9.0 for Ca^{2+}-bound PA and 20 mM glycine-KOH, pH 9.2, 1 mM EDTA for apo-PA. *Dotted black curve* corresponds to the heat capacity of the fully unfolded protein, as estimated according to ref. [16].

Table 3
Thermodynamic parameters of thermal denaturation of various states of rat β-PA estimated from the DSC data shown in Fig. 1 according to the *cooperative two-state* model [I]: mid-transition temperature (T_0), enthalpy of protein denaturation at temperature T_0 (ΔH_0), heat capacity change accompanying the transition (ΔC_p), and number of molecules involved in the transition (n).

Protein	Protein state	T_0, °C	ΔH_0, J/g	ΔC_p, J/(g·K)	N[a]
rWT β-PA	apo	30.7	11.3	0.59	0.83
	Ca^{2+}	89.3	52.9	−0.31	0.77
rWT His-tag β-PA	apo	33.3	9.5	0.59	1.04
	Ca^{2+}	93.8	23.9	−1.03	1.24

[a] n value is used as an additional fitting parameter.

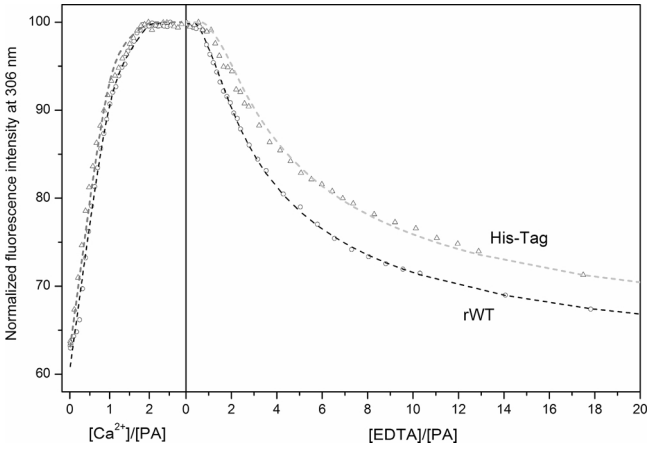

Fig. 3. Spectrofluorometric Ca^{2+}- and EDTA-titration of rat rWT β-PA and its His-tagged mutant rWT His-tag β-PA at 20 °C. Points are experimental, dashed curves are theoretical fits computed according to the *sequential metal-binding schemes* [II] and [III] (see Table 4), considering the competition between the protein and EDTA for Ca^{2+}. Intrinsic tyrosine fluorescence was excited at 275 nm. Buffer conditions: 10 mM HEPES-KOH, pH 8.2. Protein concentration was.10–16 μM.

Fig. 3 shows the results of spectrofluorimetric Ca^{2+}- and EDTA-titration of rat rWT β-PA and its His-tagged mutant rWT His-tag β-PA. Points are experimental data, whereas dashed lines are theoretical fits

Table 4
The values of equilibrium Ca^{2+} and Mg^{2+} association constants at 20 °C for untagged and His-tagged rat β-PA, estimated from the fluorimetric titrations data (Fig. 2) according to the *sequential metal-binding schemes* [II] and [III]. Protein concentration was 10–16 μM. Buffer conditions: 10 mM HEPES-KOH, pH 8.2. The accuracy of the K_{a1} and K_{a2} estimates was about ± 1/4 orders of their magnitudes.

Ca^{2+}-binding		
Protein form	$logK_1$	$logK_2$
rWT β-PA	9.0	7.3
rWT His-tag β-PA	8.9	7.1

computed according to the *sequential metal-binding scheme*, considering the competition between the protein and EDTA for Ca^{2+} (schemes II and III). The results of this fining collected in Table 4 show that the attachment of His-tag to rat β-PA slightly decreases its affinity to Ca^{2+}. However, one should keep in mind that the corresponding change is practically within the accuracy of the binding constants evaluation.

To understand how grafting of the His-tag affects intrinsic disorder predisposition of rat β-PA, we utilized a set of per-residue disorder predictors of PONDR® family (PONDR® VLXT, PONDR® VL3, PONDR® VSL2, and PONDR® FIT) access to which was provided by the DisProt database (http://original.disprot.org/) [41]. We also used IUPred platform [25] to evaluate predisposition of these proteins to have short and long intrinsically disordered regions. Results of these analyses are presented in Fig. 4. In line with previous reports [20,27,28], this multiparametric analysis of the intrinsic disorder predisposition of rat WT β-PA revealed that both N- and C-terminal regions of this protein (residues 1–19 and 76–108) are expected to be disordered, with C-tail being more disordered (see Fig. 4A). Fig. 4B shows that the His-tag grafting noticeably increased intrinsic disorder predisposition of the rat β-PA C-tail (residues 76–116), which is a rather expected output, since of the eight His-tag residues (Leu-Glu-His-His-His-His-His-His), seven (Glu-His-His-His-His-His-His) belong to the category of disorder-promoting residues [42–44]. It is likely that this increase in the intrinsic disorder content from 48.1% in rat WT β-PA to 51.7% in WT His-tag β-PA can be responsible for the reported His-tag-induced decrease in protein compaction. Finally, utilization of the ANCHOR algorithm revealed that the addition of His-tag increased the disorder-based interactivity of parvalbumin. In fact, although only two MoRFs were found in rat rWT β-PA (residues 17–18 and 98–104), its His-tagged mutant rWT His-tag β-PA was predicted to have three such disorder-based binding sites (residues 16–19, 83–91, and 96–116). These observations suggested that grafting of His-tag to the intrinsically disordered C-tail can modulate functionality of rat rWT β-PA.

Some other researchers studied effects of His-tag attachment on properties of various proteins. For example, Carson et al. (2007) surveyed and compared crystal structures of proteins with and without His tags [45]. They showed that these purification tags generally have no significant effect on the structure of the native protein: resolution and R factors are not affected, but the overall B factors are slightly higher. Chen et al. (2015) found that His-tag has no effect on polymeric state, optimal temperature and optimal pH of chondroitinase ABC I but it has little negative impact on specific enzyme activity, k_{cat}/K_m and its secondary-structure [46]. Zhao et al. (2015) solved structures of the catalytic N-acetyltransferase (NAT) domain of the bifunctional N-acetyl-L-glutamate synthase/kinase (NAGS/K) from Xylella fastidiosa bound to N-acetyl-L-glutamate (NAG) with and without an N-terminal His tag and refined them at 1.7 and 1.4 Å resolution, respectively [47]. These authors found that the His tag does not generally affect the structure. The structural differences between xfNAT-His-tag and xfNAT are comparable to the structural differences among the different subunits in the crystallized forms of both xfNAT-ht and xfNAT [47]. Zhao and Huang (2016) studied effects of His-tag on properties and structure of a Zn-finger protein ZNF191(243–368) using spectroscopic techniques and

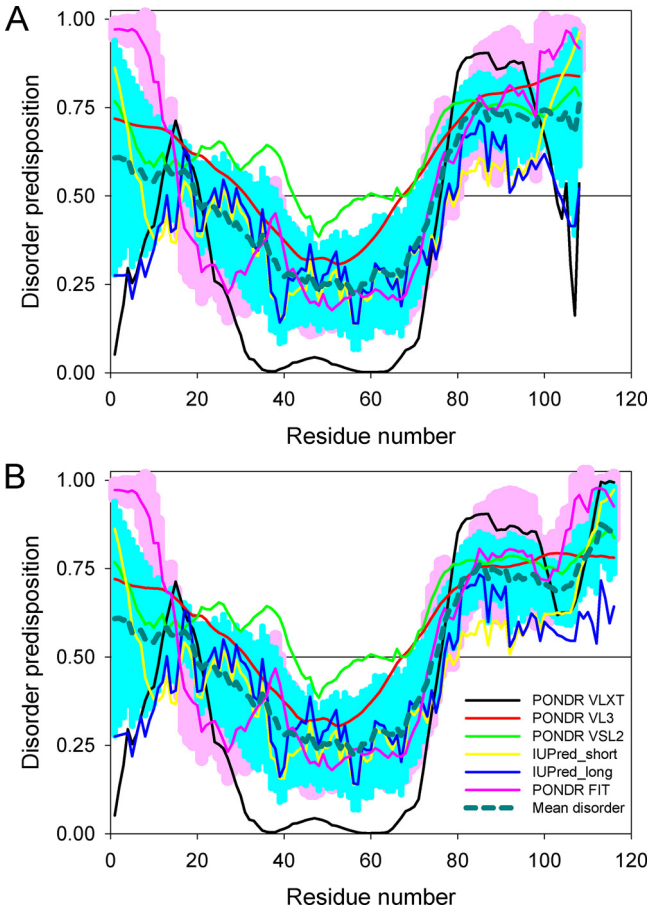

Fig. 4. Evaluating intrinsic disorder propensity of the rWT β-PA (UniProt ID: P02631) (**A**) and its His-tagged form rWT His-tag β-PA containing residues Leu-Glu-His-His-His-His-His-His at the end of the C-tail (**B**). Disorder propensities were evaluated by PONDR® VLXT (black curves), PONDR® VL3 (red curves), PONDR® VSL2 (green curves), PONDR® FIT (pink curves), IUPred_short (yellow curves), and IUPred_long (blue curves). Mean disorder predisposition was calculated by averaging of all predictor-specific per-residue disorder profiles (bold, dashed, dark cyan curves). Light pink shadow around the PONDR® FIT curve represents error distribution for this predictor, whereas light blue shadow around the mean disorder curve show distribution of standard deviations (For interpretation of the references to colour in this figure legend, the reader is referred to the web version of this article).

hydrolase experiment [48]. They found that insertion of a His-tag at the N-terminal or C-terminal end of ZNF191(243–368) has different effects on the protein. Furthermore, they revealed that ZNF191(243–368)-His_8 does not have the original structure with zinc ion coordination because eight continuous histidines at the C-terminal end hinder the normal coordination of peptide chain with zinc ions [48]. Thielges et al. (2011) found that attachment of a His tag to the N terminus of myoglobin leads to only minor changes in the electrostatic environment of the heme pocket [49]. Experiments employing 2D IR vibrational echo spectroscopy of the heme bound CO, however, revealed that significant changes occur in the short time scale (ps) dynamics of myoglobin as a result of His tag incorporation. The His tag mainly reduces the dynamics on the 1.4 ps timescale and also alters protein motions of myoglobin on the slower, > 100 s ps timescale. The results suggest that affinity tags may have effects on protein function.

The results of the present work clearly show that His-tag can seriously affect physical properties of the EF-hand protein family proteins. The attachment of His-tag to β-parvalbumin increases its α-helical content and decreases β-sheets and β-turns content of the metal free (apo-) state and decreases α-helical content by more than 10% and increases content of β-sheets and β-turns of the Ca^{2+}-loaded state. The attachment of His-tag practically does not change mean hydrodynamic radius of Ca^{2+}-loaded rat β-PA but shifts thermal unfolding peaks of both apo- and Ca^{2+}-loaded states towards higher temperatures by 3–4 °C and slightly decreases Ca^{2+} affinity of β-PA. These results should be taken into consideration in the use of His-tagged parvalbumins.

Conflict of interest

We, Alisa A. Vologzhannikova, Polina A. Khorn, Alexei S. Kazakov, Eugene A. Permyakov, Vladimir N. Uversky, and Sergei E. Permyakov, authors of the manuscript entitled “Effects of His-tags on physical properties of parvalbumins”, wish to confirm that there are no known conflicts of interest associated with this publication and there has been no significant financial support for this work that could have influenced its outcome.

Acknowledgements

This study was funded by the Russian Science Foundation (grant #16-14-10373 to E.A.P.). Part of the study was supported by grant from the Program of the Russian Academy of Sciences «Molecular and Cellular Biology»

References

[1] E. Hochuli, W. Bannwarth, H. Dobeli, R. Gentz, D. Stuber, Genetic approach to facilitate purification of recombinant proteins with a novel metal chelate adsorbent, BioTechnol 6 (1988) 1321–1325.
[2] P.N. Hengen, Methods and reagents - purification of his-tag fusion proteins from escherichia-coli, Trends Biochem. Sci. 20 (1995) 285–286.
[3] S.T. Loughran, D. Walls, Purification of poly-histidine-Tagged proteins, Methods Mol. Biol. 681 (2011) 311–335.
[4] C. Wang, B. Feng, [Research progress on site-oriented and three-dimensional immobilization of proteins], Mol. Biol. (Mosk) 49 (2015) 3–25.
[5] E.A. Permyakov, Parvalbumin, Nova Science Publishers, New York, 2006.
[6] E.A. Permyakov, Metalloproteomics, A John Wiley & Sons, Inc., Hoboken, New Jersey, 2009.
[7] E.A. Permyakov, R.H. Kretsinger, Calcium Binding Proteins, A John Wiley & Sons, Inc, Hoboken, New Jersey, 2011.
[8] A.A. Vologzhannikova, P.A. Khorn, A.S. Kazakov, R.G. Ismailov, A.S. Sokolov, V.N. Uversky, E.A. Permyakov, S.E. Permyakov, In search for globally disordered apo-parvalbumins: case of parvalbumin beta-1 from coho salmon, Cell Calcium 67 (2017) 53–64.
[9] A.S. Kazakov, A.S. Sokolov, A.A. Vologzhannikova, M.E. Permyakova, P.A. Khorn, R.G. Ismailov, K.A. Denessiouk, A.I. Denesyuk, V.A. Rastrygina, V.E. Baksheeva, E.Y. Zernii, D.V. Zinchenko, V.V. Glazatov, V.N. Uversky, T.A. Mirzabekov, E.A. Permyakov, S.E. Permyakov, Interleukin-11 binds specific EF-hand proteins via their conserved structural motifs, J. Biomol. Struct. Dyn. 35 (2017) 78–91.
[10] S.E. Permyakov, A.A. Vologzhannikova, V.I. Emelyanenko, E.L. Knyazeva, A.S. Kazakov, Y.S. Lapteva, M.E. Permyakova, A.P. Zhadan, E.A. Permyakov, The impact of alpha-N-acetylation on structural and functional status of parvalbumin, Cell Calcium 52 (2012) 366–376.
[11] R.K. Scopes, Measurement of protein by spectrophotometry at 205 nm, Anal. Biochem. 59 (1974) 277–282.
[12] M. Yazawa, M. Sakuma, K. Yagi, Calmodulins from muscles of marine invertebrates, scallop and sea anemone, J. Biochem. 87 (1980) 1313–1320.
[13] H.E. Blum, P. Lehky, L. Kohler, E.A. Stein, E.H. Fischer, Comparative properties of vertebrate parvalbumins, J. Biol. Chem. 252 (1977) 2834–2838.
[14] N. Sreerama, S.Y. Venyaminov, R.W. Woody, Estimation of protein secondary structure from circular dichroism spectra: inclusion of denatured proteins with native proteins in the analysis, Anal. Biochem. 287 (2000) 243–251.
[15] M. Häckel, H.J. Hinz, G.R. Hedwig, Partial molar volumes of proteins: amino acid side-chain contributions derived from the partial molar volumes of some tripeptides over the temperature range 10-90 degrees C, Biophys. Chem. 82 (1999) 35–50.
[16] M. Häckel, H.J. Hinz, G.R. Hedwig, A new set of peptide-based group heat capacities for use in protein stability calculations, J. Mol. Biol. 291 (1999) 197–213.
[17] S.E. Permyakov, A.G. Bakunts, M.E. Permyakova, A.I. Denesyuk, V.N. Uversky, E.A. Permyakov, Metal-controlled interdomain cooperativity in parvalbumins, Cell Calcium 46 (2009) 163–175.
[18] E.A. Permyakov, V.N. Medvedkin, L.P. Kalinichenko, E.A. Burstein, Comparative study of physiochemical properties of two pike parvalbumins by means of their intrinsic tyrosyl and phenylalanyl fluorescence, Arch. Biochem. Biophys. 227 (1983) 9–20.
[19] G. Schwarzenbach, H. Flaschka, Die komplexometrische titration, Ferdinand Enke, Verlag, Stuttgart, 1965.
[20] S.E. Permyakoy, A.G. Bakunts, A.I. Denesyuk, E.L. Knyazeva, V.N. Uversky, E.A. Permyakov, Apo-parvalbumin as an intrinsically disordered protein, Proteins-

Struct. Funct. Bioinf. 72 (2008) 822–836.
[21] P. Romero, Z. Obradovic, X. Li, E.C. Garner, C.J. Brown, A.K. Dunker, Sequence complexity of disordered protein, Proteins 42 (2001) 38–48.
[22] K. Peng, P. Radivojac, S. Vucetic, A.K. Dunker, Z. Obradovic, Length-dependent prediction of protein intrinsic disorder, BMC Bioinf. 7 (2006) 208.
[23] Z. Obradovic, K. Peng, S. Vucetic, P. Radivojac, C.J. Brown, A.K. Dunker, Predicting intrinsic disorder from amino acid sequence, Proteins 53 (Suppl 6) (2003) 566–572.
[24] B. Xue, R.L. Dunbrack, R.W. Williams, A.K. Dunker, V.N. Uversky, PONDR-FIT: a meta-predictor of intrinsically disordered amino acids, Biochim. Biophys. Acta 1804 (2010) 996–1010.
[25] Z. Dosztanyi, V. Csizmok, P. Tompa, I. Simon, IUPred: web server for the prediction of intrinsically unstructured regions of proteins based on estimated energy content, Bioinformatics 21 (2005) 3433–3434.
[26] Z. Dosztanyi, V. Csizmok, P. Tompa, I. Simon, The pairwise energy content estimated from amino acid composition discriminates between folded and intrinsically unstructured proteins, J. Mol. Biol. 347 (2005) 827–839.
[27] S.E. Permyakov, A.A. Vologzhannikova, P.A. Khorn, M.P. Shevelyova, A.S. Kazakov, V.I. Emelyanenko, A.I. Denesyuk, K. Denessiouk, V.N. Uversky, E.A. Permyakov, Comprehensive analysis of the roles of' black' and' gray' clusters in structure and function of rat beta-parvalbumin, Cell Calcium 75 (2018) 64–78.
[28] E.I. Deryusheva, A.I. Denesyuk, K. Denessiouk, V.N. Uversky, S.E. Permyakov, E.A. Permyakov, On the relationship between the conserved' black' and' gray' structural clusters and intrinsic disorder in parvalbumins, Int. J. Biol. Macromol. 120 (2018) 1055–1062.
[29] I. Walsh, M. Giollo, T. Di Domenico, C. Ferrari, O. Zimmermann, S.C. Tosatto, Comprehensive large-scale assessment of intrinsic protein disorder, Bioinformatics 31 (2015) 201–208.
[30] X. Fan, L. Kurgan, Accurate prediction of disorder in protein chains with a comprehensive and empirically designed consensus, J. Biomol. Struct. Dyn. 32 (2014) 448–464.
[31] Z. Peng, L. Kurgan, On the complementarity of the consensus-based disorder prediction, Pacific Symposium on Biocomputing, Pac. Symp. Biocomput. (2012) 176–187.
[32] C.J. Oldfield, Y. Cheng, M.S. Cortese, P. Romero, V.N. Uversky, A.K. Dunker, Coupled folding and binding with alpha-helix-forming molecular recognition elements, Biochemistry 44 (2005) 12454–12470.
[33] A. Mohan, C.J. Oldfield, P. Radivojac, V. Vacic, M.S. Cortese, A.K. Dunker, V.N. Uversky, Analysis of molecular recognition features (MoRFs), J. Mol. Biol. 362 (2006) 1043–1059.
[34] V. Vacic, C.J. Oldfield, A. Mohan, P. Radivojac, M.S. Cortese, V.N. Uversky, A.K. Dunker, Characterization of molecular recognition features, MoRFs, and their binding partners, J. Proteome Res. 6 (2007) 2351–2366.
[35] Y. Cheng, C.J. Oldfield, J. Meng, P. Romero, V.N. Uversky, A.K. Dunker, Mining alpha-helix-forming molecular recognition features with cross species sequence alignments, Biochemistry 46 (2007) 13468–13477.
[36] A.K. Dunker, Z. Obradovic, The protein trinity–linking function and disorder, Nat. Biotechnol. 19 (2001) 805–806.
[37] H.J. Dyson, P.E. Wright, Coupling of folding and binding for unstructured proteins, Curr. Opin. Struct. Biol. 12 (2002) 54–60.
[38] V.N. Uversky, C.J. Oldfield, A.K. Dunker, Showing your ID: intrinsic disorder as an ID for recognition, regulation and cell signaling, J. Mol. Recognit. 18 (2005) 343–384.
[39] B. Meszaros, I. Simon, Z. Dosztanyi, Prediction of protein binding regions in disordered proteins, PLoS Comput. Biol. 5 (2009) e1000376.
[40] Z. Dosztanyi, B. Meszaros, I. Simon, ANCHOR: web server for predicting protein binding regions in disordered proteins, Bioinformatics 25 (2009) 2745–2746.
[41] D. Piovesan, F. Tabaro, I. Micetic, M. Necci, F. Quaglia, C.J. Oldfield, M.C. Aspromonte, N.E. Davey, R. Davidovic, Z. Dosztanyi, A. Elofsson, A. Gasparini, A. Hatos, A.V. Kajava, L. Kalmar, E. Leonardi, T. Lazar, S. Macedo-Ribeiro, M. Macossay-Castillo, A. Meszaros, G. Minervini, N. Murvai, J. Pujols, D.B. Roche, E. Salladini, E. Schad, A. Schramm, B. Szabo, A. Tantos, F. Tonello, K.D. Tsirigos, N. Veljkovic, S. Ventura, W. Vranken, P. Warholm, V.N. Uversky, A.K. Dunker, S. Longhi, P. Tompa, S.C. Tosatto, DisProt 7.0: a major update of the database of disordered proteins, Nucleic Acids Res. (2017) 45D1123-d1124.
[42] A. Campen, R.M. Williams, C.J. Brown, J. Meng, V.N. Uversky, A.K. Dunker, TOP-IDP-scale: a new amino acid scale measuring propensity for intrinsic disorder, Protein Pept. Lett. 15 (2008) 956–963.
[43] V. Vacic, V.N. Uversky, A.K. Dunker, S. Lonardi, Composition Profiler: a tool for discovery and visualization of amino acid composition differences, BMC Bioinf. 8 (2007) 211.
[44] A.K. Dunker, J.D. Lawson, C.J. Brown, R.M. Williams, P. Romero, J.S. Oh, C.J. Oldfield, A.M. Campen, C.M. Ratliff, K.W. Hipps, J. Ausio, M.S. Nissen, R. Reeves, C. Kang, C.R. Kissinger, R.W. Bailey, M.D. Griswold, W. Chiu, E.C. Garner, Z. Obradovic, Intrinsically disordered protein, J. Mol. Graph. Model. 19 (2001) 26–59.
[45] M. Carson, D.H. Johnson, H. McDonald, C. Brouillette, L.J. DeLucas, His-tag impact on structure, Acta Crystallogr D 63 (2007) 295–301.
[46] Z.Y. Chen, Y. Li, Q.P. Yuan, Study the effect of His-tag on chondroitinase ABC I based on characterization of enzyme, Int. J. Biol. Macromol. 78 (2015) 96–101.
[47] G.X. Zhao, Z.M. Jin, N.M. Allewell, M. Tuchman, D.S. Shi, Structures of the N-acetyltransferase domain of Xylella fastidiosa N-acetyl-L-glutamate synthase/kinase with and without a his tag bound to N-acetyl-L-glutamate, Acta Crystallogr. F 71 (2015) 86–95.
[48] D.X. Zhao, Z.X. Huang, Effect of his-tag on expression, purification, and structure of zinc finger protein, ZNF191(243-368), Bioinorg. Chem. Appl. (2016).
[49] M.C. Thielges, J.K. Chung, J.Y. Axup, M.D. Fayer, Influence of histidine tag attachment on picosecond protein dynamics, BiochemistryUs 50 (2011) 5799–5805.